metals

MDPI

Article

Application of the Constitutive Model in Finite Element Simulation: Predicting the Flow Behavior for 5754 Aluminum Alloy during Hot Working

Changqing Huang [1,2,3,*] and Leilei Liu [1,2]

[1] Light Alloy Research Institute, Central South University, Changsha 410083, China; 153812016@cus.edu.cn
[2] State Key Laboratory of High-performance Complicated Manufacturing, Central South University, Changsha 410083, China
[3] School of Mechanical and Electrical Engineering, Central South University, Changsha 410083, China
* Correspondence: huangcq64@csu.edu.cn; Tel.: +86-731-8887-6183

Received: 4 August 2017; Accepted: 25 August 2017; Published: 28 August 2017

Abstract: The flow behavior of 5754 aluminum alloy was researched using the plane strain compression test for the range of 300–500 °C and 0.1–10 s^{-1}. The experimental flow curves acquired directly from Gleeble-3500 show that deformation parameters have a significant effect on the flow curves. All curves show a broad peak due to the dynamic softening after the work hardening. In addition, the flow curves display a slight downward trend after reaching the peak stress at low and medium strain rates. This softening mechanism has been further investigated by the work hardening rate and the results show that the flow characteristics of 5754 aluminum alloy are mainly controlled by the mechanism of competition between hardening, dynamic recovery and continuous dynamic recrystallization. Based on the corrected true strain-stress curves, the constitutive model of the corresponding softening mechanism has been established by a linear regression method. Then, the developed model was embedded in the finite element (FE) analysis software (ABAQUS) by encoding the UHARD subroutine and the hot compression process of the alloy was simulated and analyzed. The simulation results show that the sample has an uneven flow in the deformation zone, which is consistent with the grain morphology of the corresponding region of the test sample. In addition, the simulated load-stroke values were well fitted to the experimental data. The predictive ability of the model was quantified by statistical indicators. It emerged that the FE of the embedded constitutive model effectively simulates the hot working process of 5754 aluminum alloy, which has reference value for actual processing.

Keywords: hot compression; flow behavior; dynamic softening; constitutive model; finite element; subroutine

1. Introduction

Hot working as the upstream process of cold working is a very complicated and important process [1–4], which requires not only a certain dimensional accuracy, but also the need to achieve the appropriate microstructures and mechanical properties. Hence, it is essential to determine the softening mechanism and flow behavior of the metal during hot working [5], which can also provide the basis for the optimization of process parameters and related settings. The flow stress, which is an important factor to describe material dynamic response changes with processing parameters during hot deformation. Therefore, flow stress has received more attention in the field of real processing and numerical simulation [6,7]. Normally, the relationship between the strain, temperature and strain rate and flow stress of material is expressed by a constitutive model [8,9]. Nevertheless, related studies have shown that the hot working behavior of metals is accompanied by metallurgical phenomena, including dynamic softening and work hardening. Therefore, it is necessary to establish

a constitutive model reflecting the corresponding softening mechanism. This constitutive model, expressed as a specific mathematical relationship, can well describe the flow behavior of the material and can be easily applied. For the finite element method (FEM) widely used in hot working analysis and optimization [10,11], the constitutive model of metal can be encoded into the relevant analysis software to define the material flow characteristics at various strain rates and deformation temperatures [12]. The use of the constitutive model embedded in the analysis software allows the simulation to fully describe the hot working behavior of the material [12,13], which can then provide reliable reference information for actual hot working to improve the process [14]. For example, Svyetlichnyy et al. [15] developed the constitutive model of materials into FEM, and carried out a numerical simulation of the formation process of the corresponding material. However, the material library of existing finite element software lacks the 5754 aluminum alloy so that the numerical simulation of the alloy is usually replaced by an approximate material. Therefore, the simulation results do not truly reflect the flow behavior of the material.

Aluminum alloy 5754 has a high corrosion resistance, which shows wide application potential in the inner panels of the automobile structure. Its formability issues at room temperature restrict its application in this field. Hence, hot working operations are commonly applied to resolve these issues. Abbasi and Shokuhfar [16] and Lin et al. [17] pointed out that the hot working process parameters directly affect the mechanical properties of the product, which can be optimized by studying the flow behavior of materials. Hence, studying the rheological behavior of this alloy during the hot working is an important task.

In this study, a plane strain compression test was performed on a Gleeble-3500 to obtain the flow curves of the 5754 aluminum alloy at strain rates of 0.01–10 s^{-1} and deformation temperatures of 300–500 °C. The obtained flow curves were used to study the rheological behavior of the material and to establish the corresponding constitutive model. Then, the developed model was encoded into the UHARD subroutine of ABAQUS software (6.14 release, Dassault Systèmes Simulia Corp., Providence, RI, USA, 2014) using Fortran. The deformation process of hot compression is simulated by establishing a FE model similar to the experimental process. The reliability of the simulation results is evaluated by the experimental data, and the accuracy of the simulation results is further analyzed using the correlation coefficient (R) as well as average absolute relative error (AARE). Moreover, an OLYMPUS microscope (Olympus Corporation, Tokyo, Japan) was used to observe the grain morphology of different regions of the deformed sample to verify the reliability of the FE simulation of the flow behavior of the material.

2. Material and Experimental Procedure

In this paper, the chemical composition of 5754 aluminum alloy used in the experiment is shown in Table 1. The plane strain compression test was performed on the Gleeble-3500 (Dynamic System Institution, New York, NY, USA) to study the flow behavior. Therefore, the samples for testing were cut into a cuboid and the geometric shapes are as shown in Figure 1.

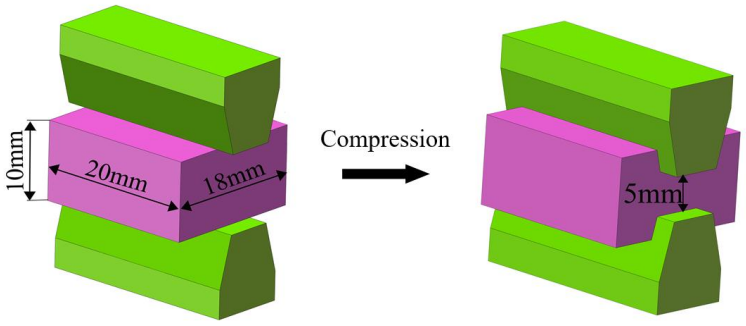

Figure 1. The geometric shape of the sample during the compression test.

The deformation conditions are as follows: strain rates were 0.1–10 s^{-1} and deformation temperatures were 300–500 °C. The Gleeble-3500 automatically records the flow curves during the test. The tantalum foils were padded between the sample and the indenter to reduce the friction. All samples were first heated to the holding temperature (500 °C) and maintained for 240 s to eliminate the thermal gradient. Then, the holding temperature is reduced to the deformation temperature (300–500 °C) to compress as shown in Figure 2. When the true strain reaches 0.7, the entire compression process ends. The sample was quenched immediately to retain deformed grain after each testing.

Table 1. Chemical composition (wt %) of 5754 aluminum alloy.

Al	Mg	Mn	Si	Fe	Gr	Zn	Cu
Bal.	2.6	0.5	0.4	0.4	0.3	0.2	0.1

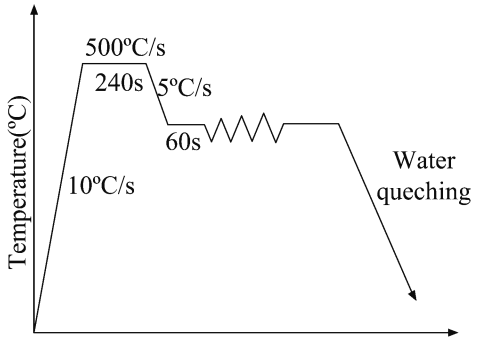

Figure 2. Hot compression process diagram.

3. Results and Discussion

3.1. Temperature Correction

The plane strain compression test was performed on the Gleeble-3500, which avoids the occurrence of the drum-like shape of the specimens. Additionally, some lubrication measures are used in hot compression. Therefore, the effect of friction on the flow curve is negligible. However, the sample is considered a non-linear power dissipater during hot compression. The dissipated power produces a certain degree of temperature rise, which results in a non-isothermal deformation process. The temperature rise can increase the softening effect, and the flow stress will be reduced accordingly. So, the temperature effect should be eliminated to ensure isothermal compression conditions. The real-time temperature and corrected flow stress can be calculated by referring to [18]. Figure 3 shows the actual value of the temperature of the specimen for isothermal plane strain compression test (PSCT). For a strain rate of 10 s^{-1}, the temperature rose to about 20 °C with respect to the preset temperature of 300 °C. Moreover, the temperature rise effect becomes weaker as the preset temperature increases. In addition, when the strain rate is less than 1, the increase in temperature is not very obvious as we can see from Figure 3. Therefore, only the high strain rate flow curves were modified. After correction of the temperature, the flow stress showed a significant increase as shown in Figure 4.

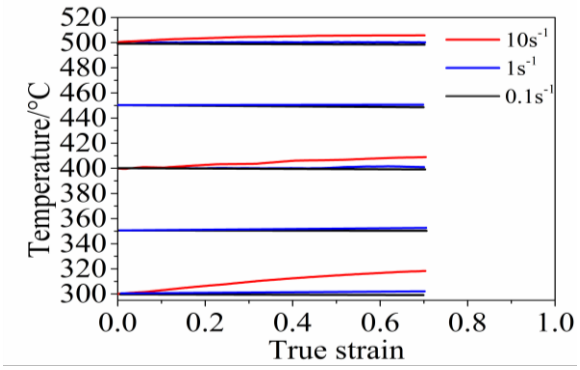

Figure 3. The true deformation temperature varying with true strain at different pre-set temperatures.

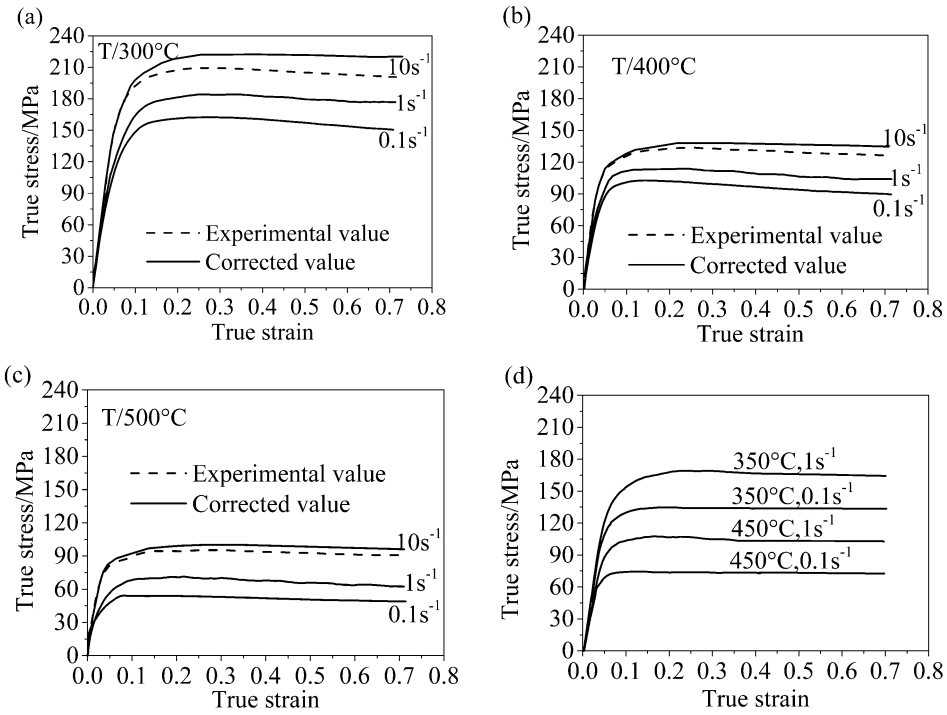

Figure 1. The experimental flow curves at different strain rates and deformation temperatures (**a**) 300 °C, (**b**) 400 °C, (**c**) 500 °C, and (**d**) 350 °C and 450 °C.

3.2. The Flow Curves of 5754 Aluminum Alloy

The corrected flow curves containing the true strain–stress data are shown in Figure 4. In the early stages, the true stress increases with the true strain due to the work hardening caused by cumulative dislocation density [19], but in the later period the flow curves rise slowly until the flow stress reaches its peak, σ_{RV}, due to the dynamic recovery (DRV) [20]. In addition, the flow curves show a slight downward trend after reaching the peak stress at strain rates of 0.1 s^{-1} and 1 s^{-1}. This phenomenon is caused by continuous dynamic recrystallization (CDRX), which is called "extended" DRV [21]. The 5754 aluminum alloy with high stacking fault energy (SFE) tends to DRV during hot deformation. The occurrence of dynamic recovery will consume accumulated dislocations, which leads to certain softening effects. Therefore, the true stress reaches its peak when the work hardening caused by the accumulated dislocations is counteracted by the softening caused by DRV. However, this does not affect the steady state of the material. As the deformation continues, DRV might gradually evolve into CDRX. Therefore, the flow curves of the high strain stage show a decreasing trend. This phenomenon is more pronounced at low and medium strain rates. Similar softening mechanisms have been reported in [21]. Moreover, the flow stress decreases with decreasing strain

rates and increasing temperature due to the low work hardening, which indicates that high temperature and low strain rate are more likely to induce softening effects.

The work hardening and dynamic softening mechanism of the alloy was further investigated by the work hardening rate (θ).

$$\theta = \frac{d\sigma}{d\varepsilon} \quad (1)$$

where σ and ε are the true stress and true plastic strain, respectively.

The true stress–work hardening rate curves are as shown in Figure 5. The hardening rate curves show that the material has significant work hardening after yielding. However, as the true stress increases, the strain hardening decreases rapidly due to the dynamic softening. All curves drop to zero after the peak true stress, indicating that the flow softening is caused by dynamic recovery [22]. However, there is a slight decrease in flow stress, which may be due to the softening of the CDRX as described above. Obviously, the θ increases with the deceasing temperature and increasing strain rate and the increasing trend is more pronounced at high stress levels, which indicates that high temperature and low strain rate are more likely to induce softening effects as described in Section 3.2.

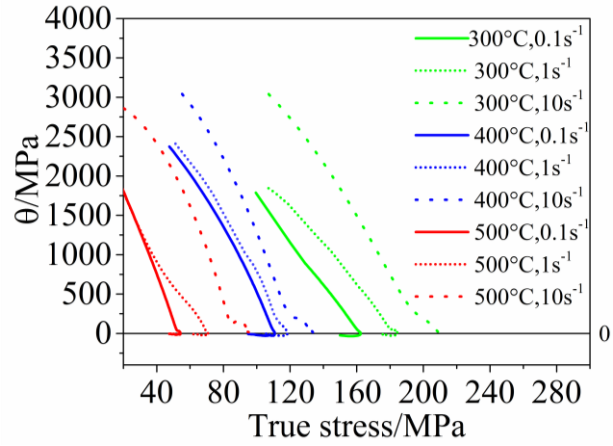

Figure 5. Work hardening rate vs. true stress of 5754 aluminum alloy.

3.3. Constitutive Model

For all stress levels, a hyperbolic sine form of the Arrhenius model (Equation (2)) can be used to predict the flow behavior of 5754 aluminum. Due to the effects of DRV and CDRX, the flow curves reach the dynamic equilibrium after the σ_{RV}. The strain has little effect on the flow stress. Therefore, the σ_{RV} is used to model and predict flow behavior.

$$\sigma(\varepsilon, \dot{\varepsilon}, T) = \sigma_{RV}(\varepsilon, \dot{\varepsilon}, T) = \frac{1}{\alpha}\sin h^{-1}[(\frac{Z}{A})^{1/n}] \quad (2)$$

where $\sigma(\varepsilon, \dot{\varepsilon}, T)$ and $\sigma_{RV}(\varepsilon, \dot{\varepsilon}, T)$ are the flow stress and constant value of flow stress for DRV curves, respectively. $\varepsilon, \dot{\varepsilon}, T$ are the strain, strain rate (s^{-1}) and absolute temperature (K), respectively. α, A and n are the constants. The effect of deformation parameters on flow stress is defined as Z (Zener–Hollomon parameter), which can be expressed as Equation (3):

$$Z = \dot{\varepsilon}\exp(Q/RT) \quad (3)$$

where Q and R represent the deformation activation energy (J mol^{-1}) and gas constant (8.31 J mol^{-1} K^{-1}), respectively.

The values of σ_{RV} which are approximately equal to the peak stresses and their corresponding strain rates and deformation temperatures obtained from the flow curves (Figure 4) are applied to

calculate the model constants. Then, all the model constants of the material have been obtained by linear regression method and the results are as shown in Table 2. Readers can refer to Reference [23–25] for more details about the identification process of material constants. The calculated n is roughly the same as that calculated in [26]. However, there are some deviations in other material constants. The calculated Q is 172.078 KJ/mol for the alloy, which is higher than that of commercial purity aluminum (105–135 KJ/mol) [5], cast A356 aluminum alloy (152–172 KJ/mol) [27] and 7050 aluminum alloy (130–153 KJ/mol) [26]. These differences are mainly due to the different material states, the content of the material element and the computational errors.

Table 2. Material constants of 5754 aluminum alloy.

Parameter	α	Q (KJ mol^{-1})	n	A
value	0.0133	172.078	5.5593	2.27×10^{11}

3.4. The Application of the Developed Model in FEM

In order to simulate the hot compression behavior of the material, the Arrhenius model is developed into the UHARD subroutine of ABAQUS using Fortran. ABAQUS provides different types of user subroutines to facilitate user simulation of complex issues including material nonlinearity and complex boundaries. The UHARD subroutine called at all materials calculation points of elements can be applied to define the yield behavior of new material. The use of the user-defined subroutine can effectively simulate the flow behavior of the material in plastic deformation. When using the UHARD subroutine, the yield stress (SYIELD), the yield stress versus the derivative of the strain (HARD(1)), the derivative of the yield stress to the strain rate (HARD(2)), and the derivative of the yield stress to the temperature (HARD(3)) need to be defined by the user. According to the established constitutive model (Equations (2) and (3)), the UHARD can be defined as follows:

$$\text{SYIELD}=\sigma(\varepsilon, \dot{\varepsilon}, T)=\frac{1}{\alpha}\sin h^{-1}\left(\frac{\dot{\varepsilon}\exp(Q/(\mathrm{R}T))}{A}\right)^{1/n} \tag{4}$$

$$X=\left(\frac{\dot{\varepsilon}\exp(Q/(\mathrm{R}T))}{A}\right)^{1/n} \tag{5}$$

$$\text{HARD}(1)=\frac{\partial\sigma(\varepsilon, \dot{\varepsilon}, T)}{\partial\varepsilon}=0 \tag{6}$$

$$\text{HARD}(2)=\frac{\partial\sigma(\varepsilon, \dot{\varepsilon}, T)}{\partial\dot{\varepsilon}}=\frac{X}{\dot{\varepsilon}\alpha n\left(1+X^2\right)^{1/2}} \tag{7}$$

$$\text{HARD}(3)=\frac{\partial\sigma(\varepsilon, \dot{\varepsilon}, T)}{\partial T}=-\frac{QX}{\mathrm{R}T^2\alpha n\left(1+X^2\right)^{1/2}} \tag{8}$$

3.5. Finite Element Model

The FE model of hot compression is as shown in Figure 6. The samples and forming tools are simultaneously heated to the same temperature to eliminate the thermal gradient during the test, as described in Section 2. Therefore, the simulation does not take into account thermal transmission of the contact surfaces. The forming tools were set as the analytical rigid surface. However, the billet is set as a three-dimensional deformed body. With the accumulation of strain, coarse grids are prone to distortion in the late stages of compression deformation, which can lead to predictive errors in the model. In order to avoid these errors due to grid distortion, the mesh of the deformed area has been

refined as shown in Figure 7. In order to achieve the same deformation rates (0.1, 1 and 10 s^{-1}) as the experiment, the stroke–time curves of the upper punch of the Gleeble-3500 (Figure 8) obtained by the test were used to define the displacement boundary of the upper-punch, and the bottom-punch was fixed.

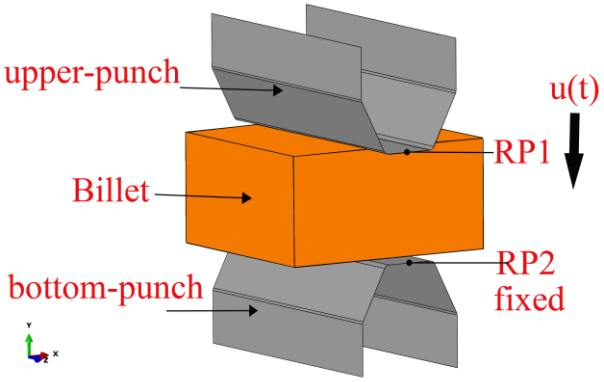

Figure 6. The FE model of the hot compression test.

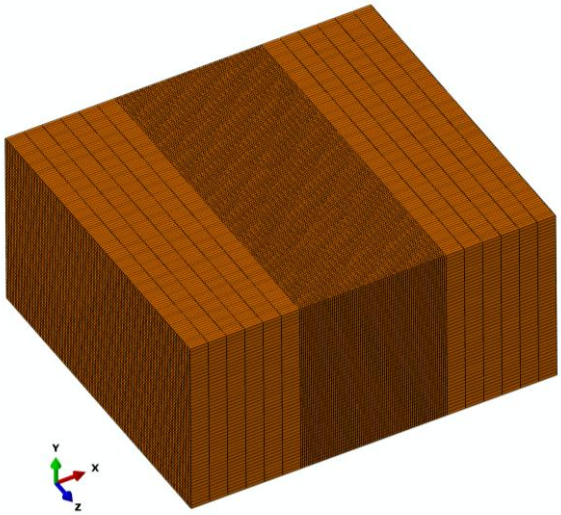

Figure 7. The refined grid of the deformation body.

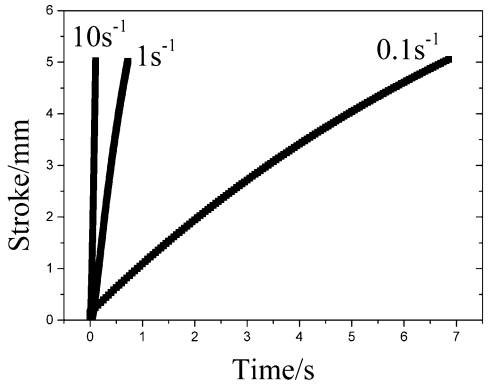

Figure 8. The stroke curves of the upper punch of the Gleeble-3500.

The simulation results at a strain rate of 0.1 s^{-1} and a deformation temperature of 300 °C are shown in Figure 9. It can be seen from Figure 9a that uneven deformation occurs in the deformation zone of the specimen. The equivalent plastic strain (PEEQ) of the central region (C) of the sample reaches the maximum value of 1.35, whereas the PEEQ of the surface region (A and B) in contact

with the dies is small. The PEEQ at B is almost zero, although the overall average strain is 0.7. Figure 9b shows the mises stress distribution of the specimen. It can be seen that the stress in the deformed region is relatively uniform (σ_{RV}), although the strain (as shown in Figure 9a) is not uniform. This phenomenon indicates that the material has entered a steady-state flow phase caused by DRV and CDRX. Therefore, the true strain in the steady-state flow stage has little effect on the flow stress, as described in Section 3.3. It can be seen from Figure 9c that the simulated maximum principal strain rate is consistent with the experimental strain rate of 0.1 s^{-1}.

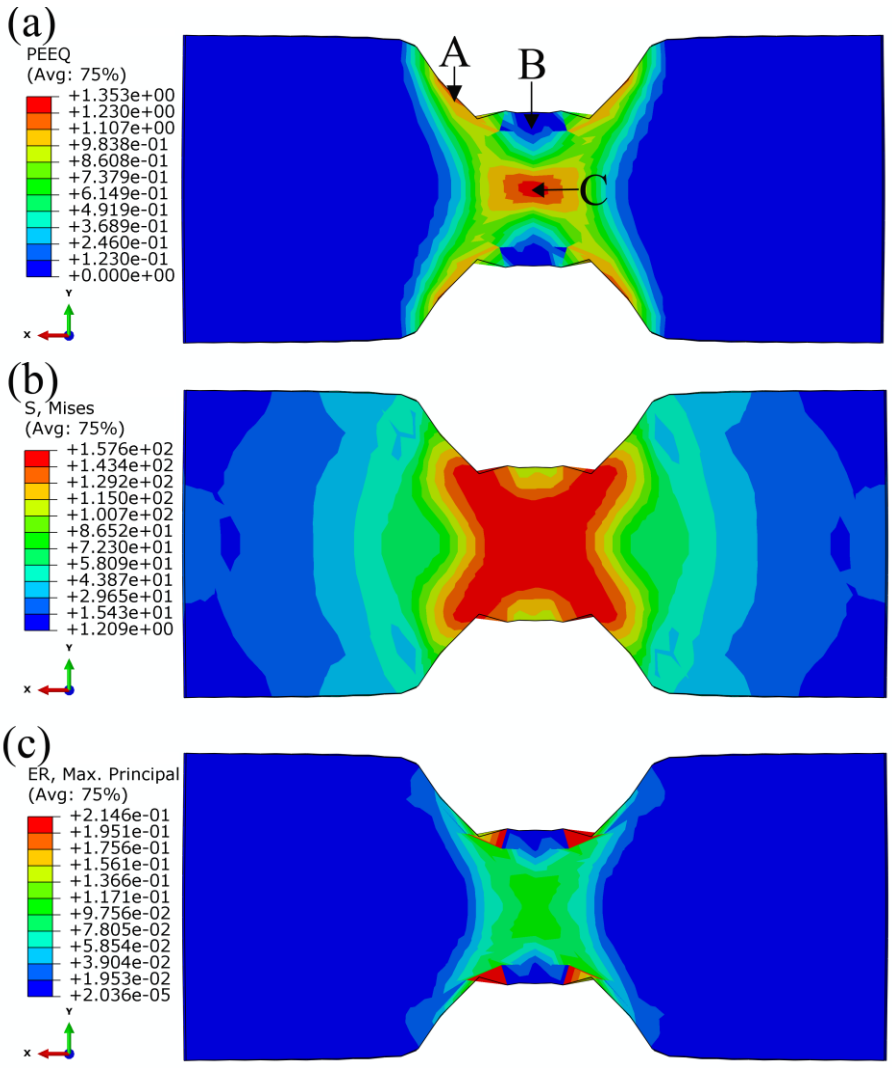

Figure 9. Distributions of equivalent plastic strain (**a**), mises stress (**b**) and maximum principal strain rate (**c**) at 300 °C and 0.1 s^{-1}.

The reliability of the simulation results is further verified by the microstructure of the deformed specimens in different regions. As shown in Figures 10 and 11, surface region B in which the sample is in contact with the upper die, holds equiaxed grains with a size of about 95 um, which is a similar size and shape to the grains of the un-deformed region A (96 um). However, the grain of the central region of the specimen is elongated in the Z direction due to strong compression in the Y direction. As can be seen from the simulation results, there is almost no plastic strain in the B region indicating that the flow of the material in this region is not very good. Therefore, this area retains the un-deformed grains. At the central region C, the sample produces the largest plastic strain, which causes the grain of the region to be compressed into a fibrous morphology. Finally, the simulated results coincide well with the observed grain morphology. In summary, the FE simulation of the embedded constitutive model can accurately describe the hot flow behavior of the material.

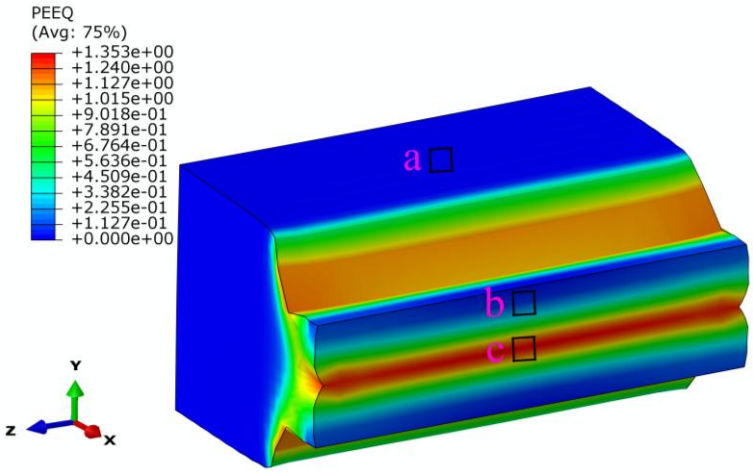

Figure 10. The distribution of equivalent plastic strain at 300 °C and 0.1 s^{-1}.

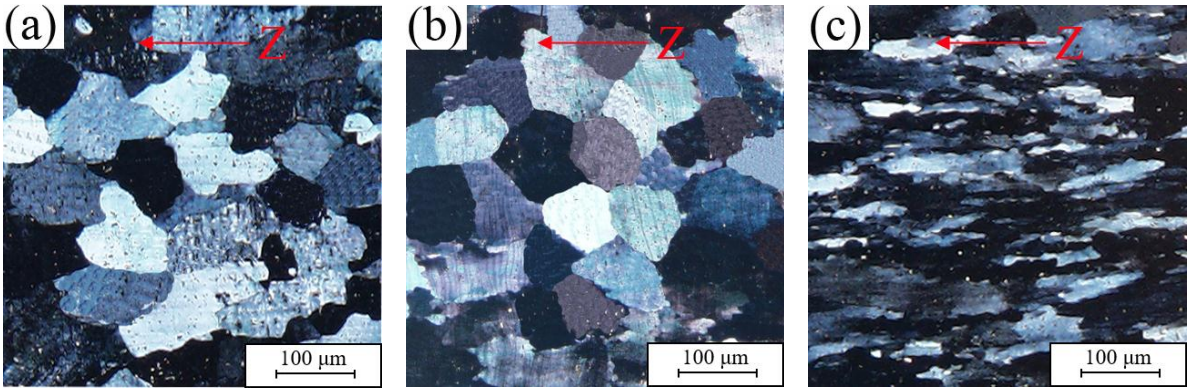

Figure 11. The distribution of the microstructure at 300 °C and 0.1 s^{-1} (**a**) region A, (**b**) region B, and (**c**) region C.

The stroke-force of the upper-punch at different strain rates and deformation temperatures is also simulated and predicted by the FEM of the embedded constitutive model. The simulated results are as shown in Figure 12. The predicted stroke-force curves agree well with the experimental data at 0.1–10 s^{-1} and 300–500 °C. The deviation between the experimental curves and the predicted curves is small. The AARE and R are often used to assess the degree of agreement between predicted and experimental values, which can be calculated by Equations (9) and (10), respectively. Normally, R is used to assess the linear correlation between the original and predicted values [28]. However, when the prediction is biased to a local range, its ability to evaluate is poor. Therefore, the unbiased statistical AARE is applied to verify the model's reliability. Then, the calculated value of R and AARE are 0.997% and 1.25%, respectively. The results indicate that the FEM of the embedded constitutive model can effectively simulate and analyze the hot working behavior of 5754 aluminum alloys, which can provide a reference for other forming processes of the alloy, such as hot rolling and forging.

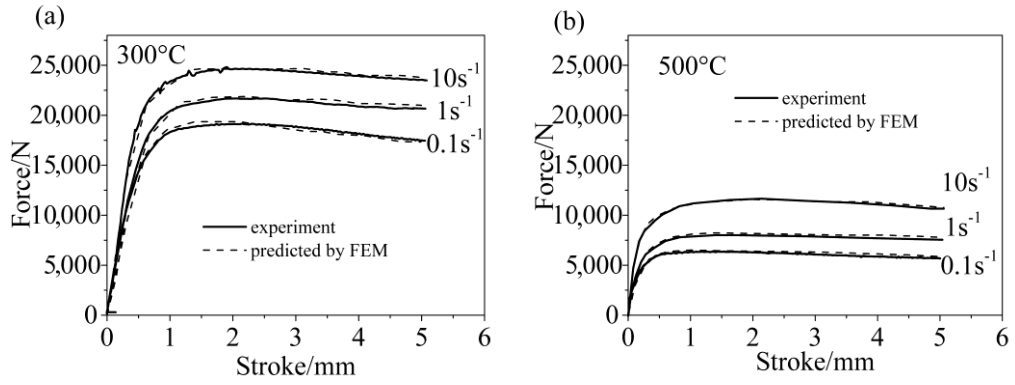

Figure 2. Comparison between predicted results by FE and experimental data. (**a**) 300 °C and (**b**) 500 °C.

$$R = \frac{\sum_{i=1}^{N}(\sigma_O^i - \overline{\sigma}_O)(\sigma_C^i - \overline{\sigma}_C)}{\sqrt{\sum_{i=1}^{N}(\sigma_O^i - \overline{\sigma}_O)^2 \sum_{i=1}^{N}(\sigma_C^i - \overline{\sigma}_C)^2}} \quad (9)$$

$$AARE(\%) = \frac{1}{N}\sum_{i=1}^{N}\left|\frac{\sigma_O^i - \sigma_C^i}{\sigma_O^i}\right| \times 100\% \quad (10)$$

where σ_O^i and σ_C^i are the experimental data and predicted data, respectively. $\overline{\sigma}_O$ and $\overline{\sigma}_C$ represent the average values of σ_O^i and σ_C^i, respectively. N represents the number of the experimental data.

4. Conclusions

The hot working behavior of 5754 aluminum alloy at strain rates of 0.1–10 s^{-1} and deformation temperatures of 300–500 °C was studied by hot compression tests and the finite element method of the embedded constitutive model. The conclusions are as follows:

(1) The strain rate and deformation temperature have significant influence on the flow behavior of 5754 aluminum alloy. The flow stress increases with increasing strain rate and decreases with increasing deformation temperature. In addition, the true stress increases with the true strain in the early stages, but in the later period, the true stress remains constant, which represents the classical characteristics of work hardening (WH) and dynamic recovery (DRV). However, the flow curves of 5754 aluminum alloy at medium and low strain rates did not reach a strict dynamic equilibrium. The flow curve decreases slightly with the increase of strain due to the CDRX (extended DRV). Meanwhile, the calculated work hardening rate shows that DRV and CDRX are the main softening mechanisms of 5754 aluminum alloy during deformation.

(2) The developed Arrhenius constitutive model of 5754 aluminum alloy is embedded in ABAQUS by encoding the UHARD subroutine to simulate the hot compression deformation.

(3) The simulated PEEQ shows that uneven deformation occurs in the deformation zone of the specimen. There is almost no plastic strain in the B region indicating that the flow of the material in this region is poor and this area still retains the un-deformed grains. At the central region C, the sample produces the largest plastic strain, which causes the grain of the region to be compressed into a fibrous morphology. The simulated results coincide well with the observed grain morphology. Therefore, the FEM simulation of the embedded constitutive model can effectively describe the flow behavior of the material.

(4) The stroke-force of the die at different strain rates and deformation temperatures is further simulated and predicted by the FEM of the embedded constitutive model. The predicted stroke-force curves agree well with the experimental data at 0.1–10 s^{-1} and 300–500 °C. Then, the predictive ability is evaluated by R and AARE and the calculated value of R and AARE are 0.997% and 1.25%, respectively. These results indicate that the FEM of the embedded

constitutive model can accurately simulate and analyze the hot working behavior of 5754 aluminum alloy, which can provide a reference for other forming processes of the alloy.

Acknowledgments: The authors appreciate financial support from the Natural Science Foundation of China under Grant 51275533 and by the State Key Laboratory of High-Performance Complex Manufacturing (Contract No. zzyjkt2013-10B), Central South University, China.

Author Contributions: Changqing Huang conceived and designed the experiments; Leilei Liu performed the experiments; Changqing Huang and Leilei Liu analyzed the data; Changqing Huang wrote the manuscript; Leilei Liu contributed to the revision of the paper.

Conflicts of Interest: The authors declare no conflict no interest.

References

1. Sellars, C.M.; Mctegart, W.J. On the mechanism of hot deformation. *Acta Metall.* **1966**, *14*, 1136–1138.
2. Changizian, P.; Zarei-Hanzaki, A.; Roostaei, A.A. The high temperature flow behavior modeling of az81 magnesium alloy considering strain effects. *Mater. Design* **2012**, *39*, 384–389.
3. Jha, J.S.; Tewari, A.; Mishra, S.; Toppo, S. Constitutive relations for Ti-6Al-4V hot working. *Procedia Eng.* **2017**, *173*, 755–762.
4. Jabbari Taleghani, M.A.; Ruiz Navas, E.M.; Salehi, M.; Torralba, J.M. Hot deformation behaviour and flow stress prediction of 7075 aluminium alloy powder compacts during compression at elevated temperatures. *Mater. Sci. Eng. A* **2012**, *534*, 624–631.
5. Rezaei Ashtiani, H.R.; Parsa, M.H.; Bisadi, H. Constitutive equations for elevated temperature flow behavior of commercial purity aluminum. *Mater. Sci. Eng. A* **2012**, *545*, 61–67.
6. Han, Y.; Qiao, G.; Sun, J.; Zou, D. A comparative study on constitutive relationship of as-cast 904l austenitic stainless steel during hot deformation based on arrhenius-type and artificial neural network models. *Comput. Mater. Sci.* **2013**, *67*, 93–103.
7. Jenab, A.; Karimi Taheri, A. Experimental investigation of the hot deformation behavior of AA7075: Development and comparison of flow localization parameter and dynamic material model processing maps. *Int. J. Mech. Sci.* **2014**, *78*, 97–105.
8. Krishnan, S.A.; Phaniraj, C.; Ravishankar, C.; Bhaduri, A.K.; Sivaprasad, P.V. Prediction of high temperature flow stress in 9Cr–1Mo ferritic steel during hot compression. *Int. J. Press. Vessels Pip.* **2011**, *88*, 501–506.
9. Phaniraj, C.; Samantaray, D.; Mandal, S.; Bhaduri, A.K. A new relationship between the stress multipliers of garofalo equation for constitutive analysis of hot deformation in modified 9Cr–1Mo (P91) steel. *Mater. Sci. Eng. A* **2011**, *528*, 6066–6071.
10. Hor, A.; Morel, F.; Lebrun, J.-L.; Germain, G. An experimental investigation of the behaviour of steels over large temperature and strain rate ranges. *Int. J. Mech. Sci.* **2013**, *67*, 108–122.
11. Ciccarelli, D.; El Mehtedi, M.; Jäger, A.; Spigarelli, S. Analysis of flow stress and deformation mechanism under hot working of ZK60 magnesium alloy by a new strain-dependent constitutive equation. *J. Phys. Chem. Solids* **2015**, *87*, 183–195.
12. Samantaray, D.; Mandal, S.; Bhaduri, A.K. Constitutive analysis to predict high-temperature flow stress in modified 9Cr–1Mo (P91) steel. *Mater. Design* **2010**, *31*, 981–984.
13. He, X.; Yu, Z.; Liu, G.; Wang, W.; Lai, X. Mathematical modeling for high temperature flow behavior of as-cast Ti–45Al–8.5Nb–(W,B,Y) alloy. *Mater. Design* **2009**, *30*, 166–169.
14. Zhou, L.; Huang, Z.Y.; Wang, C.Z.; Zhang, X.X.; Xiao, B.L.; Ma, Z.Y. Constitutive flow behaviour and finite element simulation of hot rolling of SiCp/2009Al composite. *Mech. Mater.* **2016**, *93*, 32–42.
15. Svyetlichnyy, D.; Nowak, J.; Biba, N.; Łach, Ł. Flow stress models for deformation under varying condition—Finite element method simulation. *Int. J. Adv. Manuf. Technol.* **2016**, *87*, 543–552.
16. Abbasi, S.M.; Shokuhfar, A. Prediction of hot deformation behaviour of 10Cr–10Ni–5Mo–2Cu steel. *Mater. Lett.* **2007**, *61*, 2523–2526.
17. Lin, Y.C.; Chen, M.-S.; Zhong, J. Microstructural evolution in 42CrMo steel during compression at elevated temperatures. *Mater. Lett.* **2008**, *62*, 2132–2135.
18. Chamanfar, A.; Jahazi, M.; Gholipour, J.; Wanjara, P.; Yue, S. Evolution of flow stress and microstructure during isothermal compression of waspaloy. *Mater. Sci. Eng. A* **2014**, *615*, 497–510.
19. Liao, C.-H.; Wu, H.-Y.; Lee, S.; Zhu, F.-J.; Liu, H.-C.; Wu, C.-T. Strain-dependent constitutive analysis of

extruded AZ61 Mg alloy under hot compression. *Mater. Sci. Eng. A* **2013**, *565*, 1–8.
20. Wang, Y.; Peng, J.; Zhong, L.; Pan, F. Modeling and application of constitutive model considering the compensation of strain during hot deformation. *J. Alloys Compd.* **2016**, *681*, 455–470.
21. Haghdadi, N.; Cizek, P.; Beladi, H.; Hodgson, P.D. A novel high-strain-rate ferrite dynamic softening mechanism facilitated by the interphase in the austenite/ferrite microstructure. *Acta Mater.* **2017**, *126*, 44–57.
22. Jiang, F.; Zhang, H.; Li, L.; Chen, J. The kinetics of dynamic and static softening during multistage hot deformation of 7150 aluminum alloy. *Mater. Sci. Eng. A* **2012**, *552*, 269–275.
23. Yan, J.; Pan, Q.-L.; Li, A.-D.; Song, W.-B. Flow behavior of Al–6.2Zn–0.70Mg–0.30Mn–0.17Zr alloy during hot compressive deformation based on arrhenius and ann models. *Trans. Nonferrous Metals Soc. China* **2017**, *27*, 638–647.
24. Ji, G.; Li, F.; Li, Q.; Li, H.; Li, Z. A comparative study on arrhenius-type constitutive model and artificial neural network model to predict high-temperature deformation behaviour in aermet100 steel. *Mater. Sci. Eng. A* **2011**, *528*, 4774–4782.
25. Guo, L.; Zhang, Z.; Li, B.; Xue, Y. Modeling the constitutive relationship of powder metallurgy Al–W alloy at elevated temperature. *Mater. Design* **2014**, *64*, 667–674.
26. Li, J.; Li, F.; Cai, J.; Wang, R.; Yuan, Z.; Xue, F. Flow behavior modeling of the 7050 aluminum alloy at elevated temperatures considering the compensation of strain. *Mater. Design* **2012**, *42*, 369–377.
27. Haghdadi, N.; Zarei-Hanzaki, A.; Abedi, H.R. The flow behavior modeling of cast A356 aluminum alloy at elevated temperatures considering the effect of strain. *Mater. Sci. Eng. A* **2012**, *535*, 252–257.
28. Haghdadi, N.; Zarei-Hanzaki, A.; Khalesian, A.R.; Abedi, H.R. Artificial neural network modeling to predict the hot deformation behavior of an A356 aluminum alloy. *Mater. Design* **2013**, *49*, 386–391.